Track-and-Tune Light Field Image Sensor

Vigil Varghese, *Student Member, IEEE*, Xinyuan Qian, Shoushun Chen, *Member, IEEE*,
Shen ZeXiang, Tao Jin, Liang Guozhen, and Qi Jie Wang

***Abstract*— In this paper, we present a new technique for determining the angle of incident light using an image sensor. This technique makes use of two distinct pixel types for simultaneous coarse angle estimation and fine angle detection. A new type of pixel structure, the quadrature pixel cluster is introduced, which produces response that varies linearly with incident light angle. The proposed technique greatly reduces the overall sensor complexity and is very area efficient compared with the previous work on angle detection. The sensor is fabricated in 65-nm mixed-signal CMOS process and can accurately distinguish between angles in the range from −35° to +35°.**

***Index Terms*— Angle detection, linear angle sensitive pixels, quadrature pixel cluster, light field sensor, track-and-tune angle detection, CMOS image sensor.**

I. Introduction

LIGHT field [1] at any point in space is defined as the collection of rays from all other points in space to that particular point. Light field can be mathematically described by a seven dimensional parameterized function, know as the plenoptic function [2]. This seven dimensional function describes light field in terms of intensity variations along the x and y directions, at all times (t), for all wavelengths (λ) and for all viewing directions (V_x, V_y and V_z). The 7D plenoptic function is given by Eq. (1).

$$P(x, y, \lambda, t, V_x, V_y, V_z) \tag{1}$$

For a static scene (no variations with "t") with monochromatic illumination (constant "λ"), the 7D function can be reduced to a 5D one given below:

$$P(x, y, V_x, V_y, V_z) \tag{2}$$

This 5D function can be further reduced to a 4D one by considering the fact that the radiance along any ray does not change unless blocked [3], [4]. This 4D representation can be used to completely describe any visual scene around us. Conventional image sensors sample only a 2D version of the imaging scene and hence are limited in their capabilities for post capture image processing. Extraction of the complete 4D parameters from light field allows for certain image processing capabilities such as 3D reconstruction [3]– [5], post capture refocus [5], [6], multi viewpoint rendering [3], [4] and refocusing in presence of partial occluders [6], among others. In order to faithfully reconstruct a 3D image point by means of a 2D pixel array, we need to capture the 4D light field.

Integral photography was perhaps the first method proposed to recreate a 4D light field using the direction of incoming light rays [7]. Since then, many alternative techniques have been proposed for capturing the light angle information. Prominent among them are multi-aperture based [8] and Talbot effect based [9], [10]. These techniques are typically limited by low resolution (low pixel count) due to the requirement of a large number of pixels to resolve a single 3D point.

Conventional CMOS image sensors can only detect intensity (brightness) and wavelength (color) of incident light. In order to capture angle information, photodiode in a standard imaging pixel has to be augmented with special structures such as metal gratings, micro-lenses or metal blocks. Capturing light angle opens up new avenues in areas such as 3D image capture [11], [12], post capture image refocussing [13] and depth map computation [14] in addition to the whole range of image processing capabilities that 4D light field information provides.

Through this work we propose a new technique for angle detection. This technique, called the track-and-tune angle detection, makes use of two types of pixels for angle detection. The first type, called the Quadrature Pixel Cluster (QPC), is based on the concept of metal shading [15], [16] and produces linear response proportional to angle variations, but with low sensitivity. The second type, called the Talbot pixel [9], produces precise non-linear response proportional to the angle variations. The track-and-tune technique makes use of the linear response of QPC for coarse angle detection and non-linear response of Talbot pixels for fine angle tuning. Hence, by using two different pixel types, the complexity of the angle detection process is greatly reduced, thereby decreasing the number of pixels needed for angle detection and increasing the sensor resolution.

A major advantage of the proposed method is that a single macro-pixel (comprising of 13 sub-pixels) is capable of determining the angle of a 3D point. This is in stark contrast to the earlier Talbot effect based pixel design that used 32 pixels [9] (for only horizontal and vertical directions) for producing similar results. Moreover, the technique is independent of the wavelength of incident light and consequently can be applied more reliably to natural scenes that contain objects illuminated by light of different wavelengths.

In the next section we will describe the basics of Talbot effect based pixels and analyze their response at different wavelengths through simulations. In section III, the concepts related to quadrature pixel cluster will be described along with simulations to justify the choice of various design parameters. In section IV we will introduce the track-and-tune technique for determining angles. The technique will be further elaborated with an example in section VI. In section V we will describe the sensor architecture and finally in section VI we will explain the experimental setup and present the measured results.

II. Talbot Effect Based Pixels - Fine Angle Detection

A. Theory

Talbot effect [17] relates to the self imaging property of periodic diffraction gratings. The self images are a result of Fresnel diffraction and their location was determined by Rayleigh [18] as given by Eq. (3), where d is the grating pitch and λ is the wavelength. When λ/d is small, Eq. (3) reduces to Eq. (4), which is the well know Talbot depth. Strong intensity patterns occur at depths that are half-integer multiples of the Talbot depth. The Talbot response is sensitive to the angle of incident light. This effect, known as the off-axis Talbot effect [19], forms the basis of Talbot effect based pixels.

$$z = \frac{\lambda}{1-\sqrt{1-\lambda^2/d^2}} \tag{3}$$

$$z_t = \frac{2d^2}{\lambda} \tag{4}$$

The pioneering work on angle detection, which was based on Talbot effect [9], employs two levels of diffraction gratings. The second grating is placed at a depth 'z', below the first one and is known as the analyzer grating. It is placed to either block or pass the incident light and acts as a mask. The Talbot pixels are divided into groups, with each group having 4 pixels, each with distinct offset for the secondary grating. With 'd' as the grating pitch, the secondary gratings have offsets of '0', 'd/2', 'd/4' and '3d/4'. The pixels with secondary grating offsets of '0' and 'd/2' work as a pair and those with grating offsets 'd/4' and '3d/4' work as a pair. Fig. 1 illustrates this grating configuration. The pixel responses are paired to eliminate ambiguity that arises when secondary grating with a particular offset blocks bright light at a certain angle, but passes dim light at another angle. This ineffectiveness of the Talbot pixel with only a single secondary grating without any offsets lead to incorrect results. In order to resolve this ambiguity, pixels with complementary secondary grating offsets are made to work as pairs [9].

Each Talbot pixel group is characterized by distinct directional gratings (horizontal, vertical or diagonal) and unique angle sensitivities. Talbot pixels can only produce response for

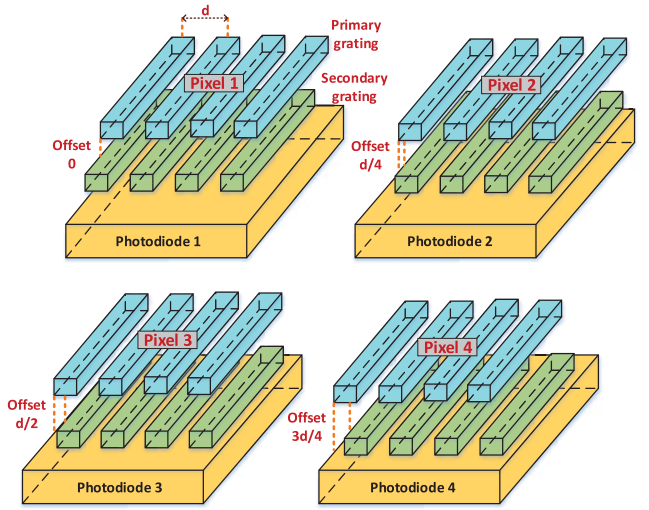

Fig. 1. Talbot pixels with secondary grating offsets of 0, d/4, d/2 and 3d/4.

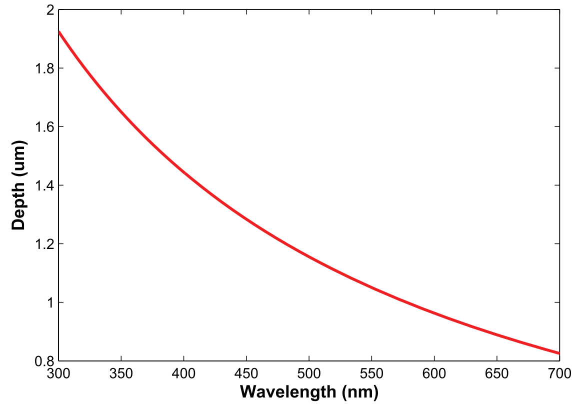

Fig. 2. Variation of half-Talbot depth, $z_t/2$, with wavelength, λ.

light source variations that are orthogonal to the grating used. Thus, in order to detect variations in horizontal direction, we need a vertical grating and vice versa. Higher angle sensitivity means large variation in response for small change in angles, but with lower range of resolvable angles. On the other hand, lower angle sensitivity means small variation in response for large change in angles, but with higher range of resolvable angles. This is a design tradeoff and cannot be eliminated. In order to overcome this limitation, earlier designs using Talbot effect based pixels used a number of pixel groups, each with distinct angle sensitivities.

One issue with Talbot pixel based design is the need to have pixel groups with different angle sensitivity values for resolving a wide enough angle range. This leads to a number of redundant pixels in the sensor, which directly translates to a large area overhead. Another issue stems directly from Eq. (4), which shows the wavelength dependence of Talbot depth. Effectiveness of the secondary grating depends heavily on the designed Talbot depth. If the wavelength varies, depth will vary, which in turn produces ambiguous results.

Fig. 2 illustrates the wavelength dependence of half-Talbot depth ($z_t/2$), where strong intensity patterns occur for a pitch of 0.76 μm. The value for pitch was calculated from Eq. 4 by

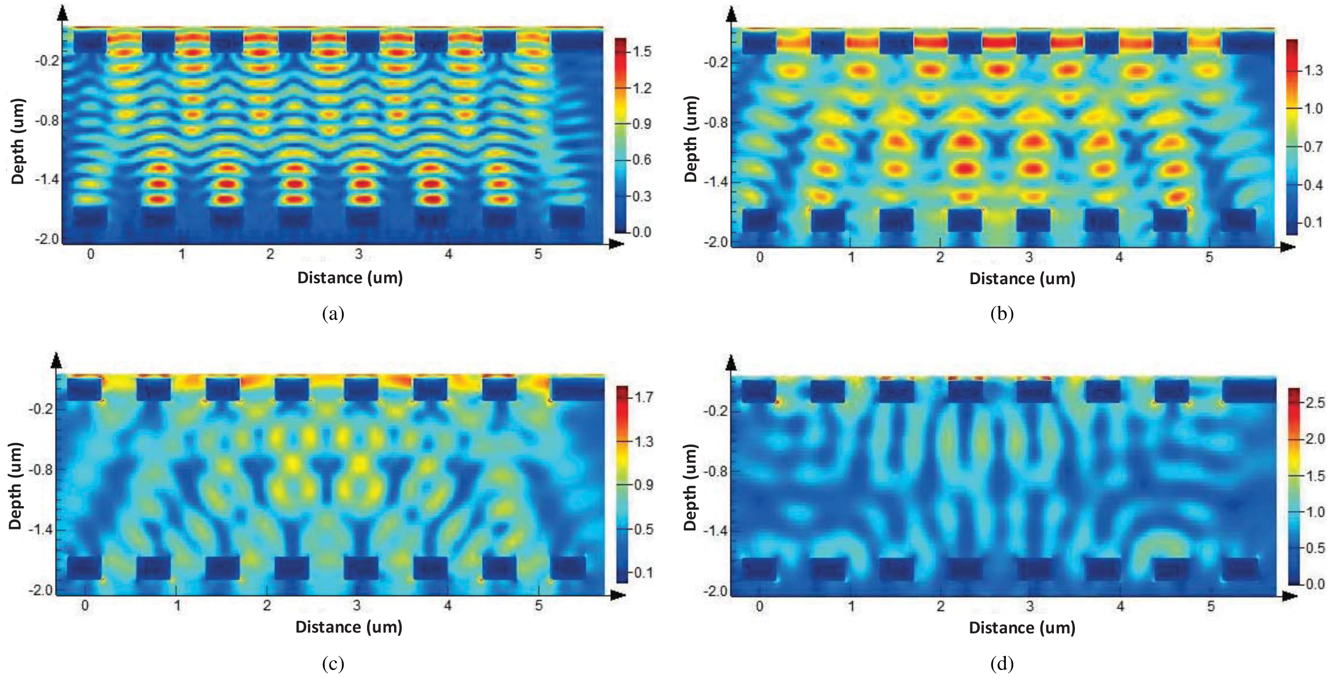

Fig. 3. Electric field profile of a single Talbot pixel with no secondary grating offset at different wavelengths for normal incidence angle (0°). (a) Wavelength of incident light, λ = 400 nm. (b) Wavelength of incident light, λ = 500 nm. (c) Wavelength of incident light, λ = 600 nm. (d) Wavelength of incident light, λ = 700 nm.

considering a wavelength of 532 nm in vacuum. For actual CMOS devices, the effective wavelength becomes 373 nm because

$$\lambda_{\text{eff}} = \frac{\lambda_{\text{vac}}}{\text{n}_{\text{ox}}} \tag{5}$$

where λ_{eff} is the wavelength of incident light in oxide, λ_{vac} is the wavelength of light in vacuum and n_{ox} is the refractive index of SiO_2 ($\text{n}_{\text{ox}} = 1.46$).

B. Simulations

For simulations a pitch of 0.76 μm with a duty cycle of 50% was used for both primary and secondary gratings. The secondary grating was placed at a depth where strong intensity patterns occurred corresponding to an effective wavelength of 373 nm (532 nm in vacuum). Fig. 4 shows the Finite Difference Time Domain (FDTD) simulation results for difference response produced by a pixel pair, such as pixel 1 and pixel 3 of Fig. 1, for plane wave illumination, as source angle is varied from $-45°$ to $+45°$. As expected, the response is cosine in nature.

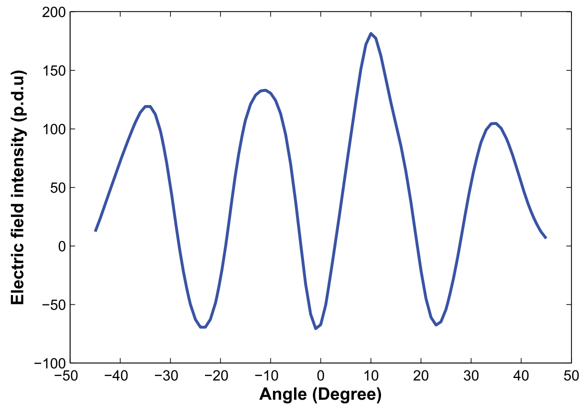

Fig. 4. FDTD simulation of difference response produced by pixel 1 and pixel 3 of Fig. 1 (λ = 400 nm).

The wavelength dependence of Talbot effect has been used in applications such as interferometry [20] to measure the step height of objects. Although it offers advantages in certain class of optical applications, for the case of angle detection it is detrimental. Fig. 3 shows the electric field profile produced by a Talbot pixel with no secondary grating offset (pixel 1 of Fig. 1) for different wavelengths at normal light incidence (0°).

In Fig. 3(a) and 3(b), the pitch is greater than the wavelengths (λ = 400 nm, 500 nm), which results in strong diffraction patterns. Whereas, in Fig. 3(c) and 3(d), the pitch is comparable to the wavelengths (λ = 600 nm, 700 nm), resulting in weak diffraction patterns. Also, at wavelengths other than the design wavelength, Talbot depth shifts resulting in a small amount of light to pass through the secondary grating. This is illustrated in Fig. 3(b), where small amounts of light leaks through the secondary grating. Only Fig. 3(a) seems to produce an ideal result corresponding to the design wavelength of 373 nm (≈400 nm).

Fig. 5 shows the Electric field intensity for different wavelengths as the light angle is varied from $-45°$ to $+45°$. We expect Fig. 5(a) to be a perfect cosine curve, since it corresponds to the design wavelength. But, we see aberrations above $+10°$ and below $-10°$. This is because of the finite number of gratings placed above the photodiode. As expected, Fig. 5(b)-5(d) show responses that are grossly inaccurate.

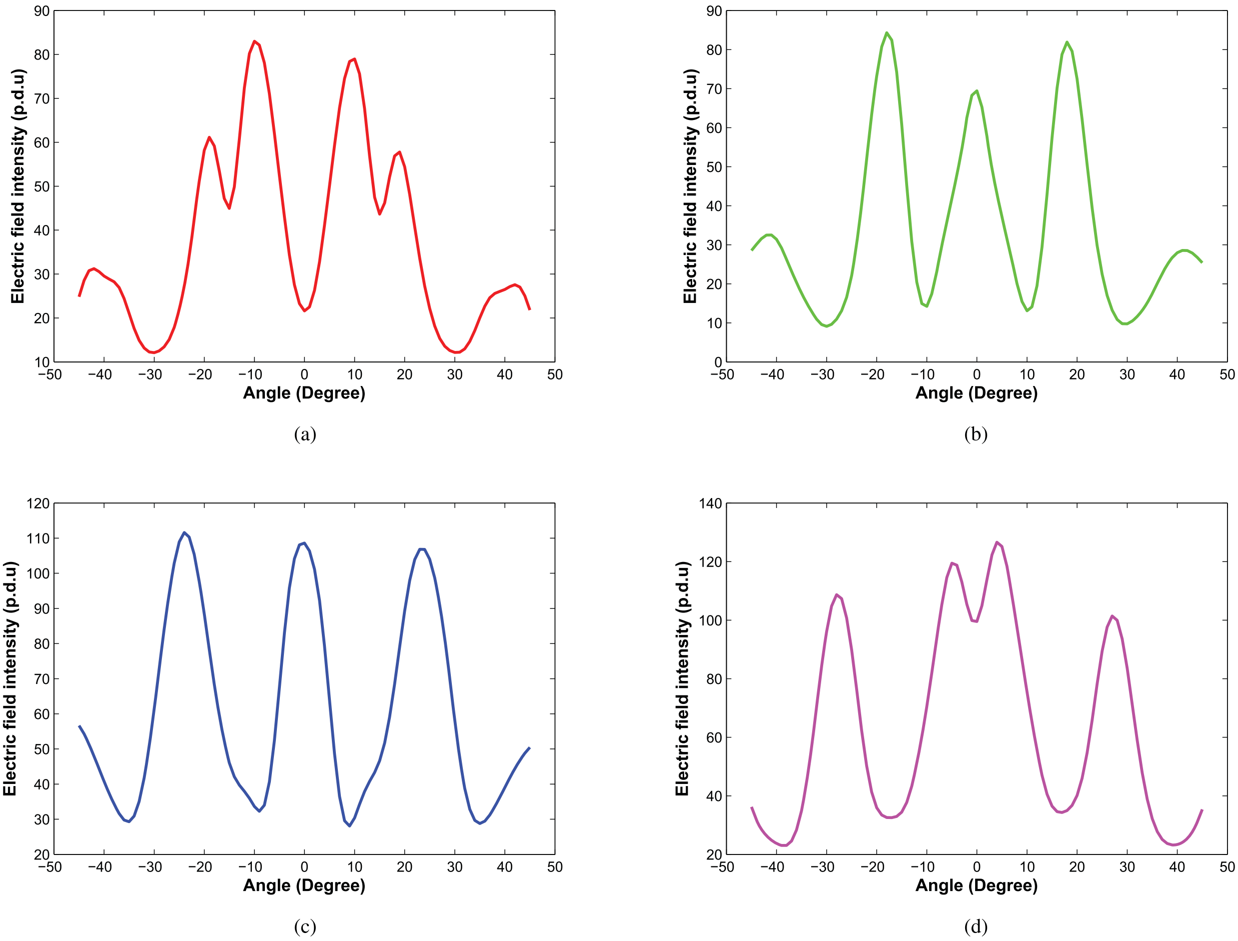

Fig. 5. Plot of electric field intensity variation of a single Talbot pixel with no secondary grating offset at different wavelengths as the incident light angle is varied from $-45°$ to $+45°$. (a) Wavelength of incident light, $\lambda = 400$ nm. (b) Wavelength of incident light, $\lambda = 500$ nm. (c) Wavelength of incident light, $\lambda = 600$ nm. (d) Wavelength of incident light, $\lambda = 700$ nm.

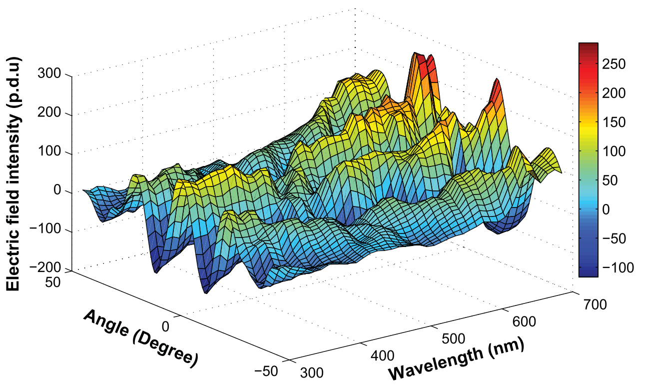

Fig. 6. Three-dimensional plot showing difference-intensity variations as a function of angle and wavelength for a pair of Talbot pixels.

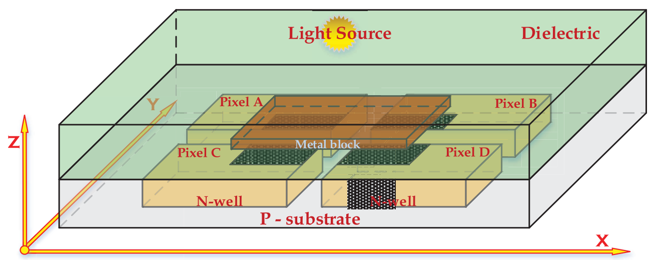

Fig. 7. Physical structure of angle sensitive quadrature pixel cluster.

Fig. 6 shows 3 dimensional variation of electric field intensity as a function of wavelength and incidence angle for the difference response produced by a pair of Talbot pixels with complementary gratings (a two dimensional case is shown in Fig. 4). As can be seen from the figure, response is symmetrical for both positive and negative angles. However, for any particular angle plane (for example take 0°), the intensity varies for different wavelengths, indicating strong wavelength dependence of Talbot pixels. Hence, Talbot pixels alone cannot be used as-is for practical applications.

III. Quadrature Pixel Cluster - Coarse Angle Detection

A. Theory

Fig. 7 shows the perspective view of the proposed structure. It consists of four photodiodes (N-well/P-sub) with a metal block on top of it. The metal block is implemented in one

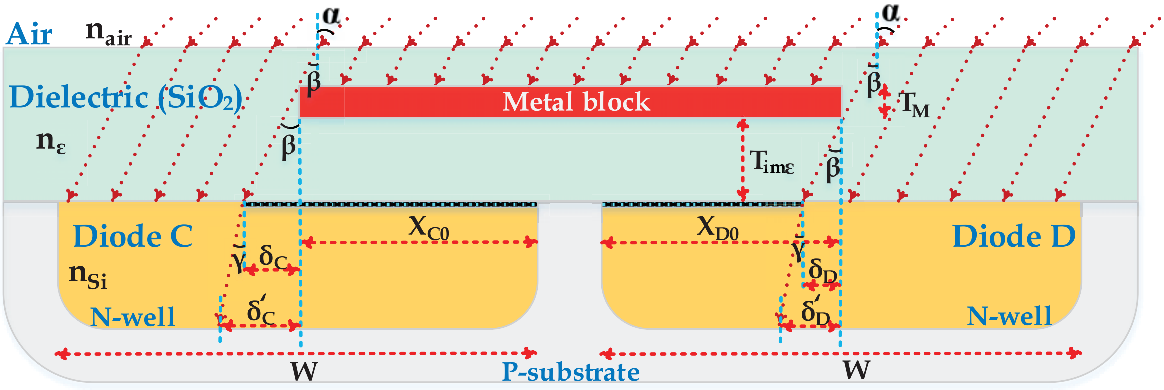

Fig. 8. 2D view of quadrature pixel cluster along the X direction.

of the layers of CMOS metal stack and partially covers the photodiodes. The area covered by the metal block is symmetrical along the X and Y directions for each of the four photodiodes. Each photodiode along with a set of transistors form the pixel.

The metal layer is present in a complex assortment of inter metal dielectrics, thin ion migration barrier layers (TiN) and SiO_2. For the sake of simplicity we consider all these dielectrics as a single dielectric having the refractive index of SiO_2.

Fig. 8 shows the two dimensional view of a QPC along the X direction. α is the incident light angle, β is the transmitted light angle at the air/SiO_2 interface and γ is the transmitted light angle at the SiO_2/Si interface. The angle γ is the one that is of interest to us, since it is this angle that determines the amount of light falling on the pn junction. However, γ is difficult to determine because of the difficulty in estimating the depth and doping of the n-well layer (doping influences the refractive index), both of which are process parameters and hence confidential.

W is the width of the photodiode and since the diode is symmetrical, its area is given by Eq. (6). X_{C0} and X_{D0} are the widths of the shaded regions of the diodes under normal illumination ($\alpha = 0°$) and the shaded areas are given by Eq. (7) and Eq. (8) respectively.

$$\mathrm{A} = W \times W \tag{6}$$
$$\mathrm{A_{shC}} = X_{C0} \times X_{C0} \tag{7}$$
$$\mathrm{A_{shD}} = X_{D0} \times X_{D0} \tag{8}$$

δ_C and δ_D are the change in the shading widths at the SiO_2/Si interface for non-normal (other than 0°) incidence of light. $\delta_C^{'}$ and $\delta_D^{'}$ are the actual shading widths at the pn junction that influence the magnitude of the photocurrent in each of the two diodes, C and D. Since γ cannot be accurately determined, the actual metal shading widths $\delta_C^{'}$ and $\delta_D^{'}$ also cannot be accurately determined. Hence $\delta_C^{'}$ and $\delta_D^{'}$ are approximated by δ_C and δ_D, which can be determined fairly accurately because β can be accurately determined. This approximation is valid because the depth of the n-well is very small compared to the dielectric stack and hence the error is very small.

Let n_{air} and n_ε be the refractive indices of air and dielectric respectively. Then, from Snell's law [21] we can write the transmitted angle β as

$$\beta = \mathrm{arcSin}(\frac{n_{air}}{n_\varepsilon}\mathrm{Sin}\alpha) \tag{9}$$

Let $T_{im\varepsilon}$ be the thickness of the inter metal dielectric stack from the bottom of the M^{th} metal layer downwards and let T_M be the thickness of the M^{th} metal layer, then the change in the shaded region, δ_C, of diode C is given by

$$\delta_C = (T_{im\varepsilon} + T_M)\tan\beta \tag{10}$$

Similarly, the change in the shaded region, δ_D, of diode D is given by

$$\delta_D = (T_{im\varepsilon})\tan\beta \tag{11}$$

Combining Eq. (9) and Eq. (10), we can write

$$\delta_C = (T_{im\varepsilon}+T_M)\tan(\mathrm{arcSin}(\frac{n_{air}}{n_\varepsilon}\mathrm{Sin}\alpha)) \tag{12}$$

Similarly, by combining Eq. (9) and Eq. (11), we can write

$$\delta_D = (T_{im\varepsilon})\tan(\mathrm{arcSin}(\frac{n_{air}}{n_\varepsilon}\mathrm{Sin}\alpha)) \tag{13}$$

Eq. (12) and Eq. (13) can be used to model a QPC and they help to determine the appropriate value of $T_{im\varepsilon}$ and T_M for an acceptable response. $T_{im\varepsilon}$ and T_M can take only a distinct set of values and are dependent on the CMOS process.

When the light angle is positive ($0° < \alpha \leq 90°$) and varies along the horizontal (X) direction (with no variation along the vertical (Y) direction), diode C is shaded more than diode D (as shown in Fig. 8) and hence light intensity recorded by diode C will be less than that recorded by diode D. The area of the shaded regions in each diode can be written as:

$$\mathrm{A_{shC}} = X_{C0} \times (X_{C0} + \delta_C) \tag{14}$$
$$\mathrm{A_{shD}} = X_{D0} \times (X_{D0} - \delta_D) \tag{15}$$

Since A is the total diode area, the area of the unshaded regions can be obtained from the following equations:

$$\mathrm{A_{ushC}} = \mathrm{A} - \mathrm{A_{shC}} \tag{16}$$
$$\mathrm{A_{ushD}} = \mathrm{A} - \mathrm{A_{shD}} \tag{17}$$

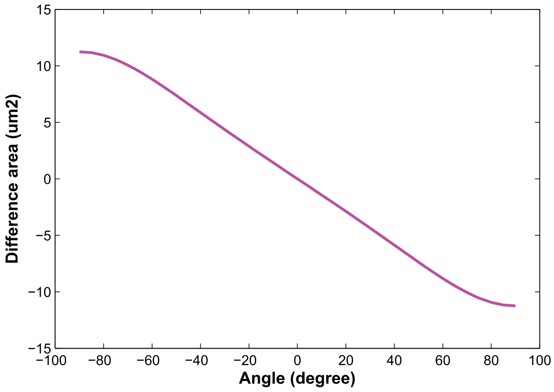

Fig. 9. Difference in unshaded area as a function of incident angle for two adjacent photodiodes in a quadrature pixel cluster.

Since A_{shD} is less than A_{shC}, A_{ushD} is greater than A_{ushC} and as a consequence diode D registers more response than diode C. For negative angles ($-90° \leq \alpha < 0°$), A_{ushD} will be lesser than A_{ushC} and hence diode C will register more response than diode D. As angle is varied from normal incidence to the maximum ($\alpha = \pm 90°$), the difference in the response produced by the diodes keep on increasing and reaches a limiting value at $\alpha = \pm 90°$. Since this difference is linear, the angle information can be decoded easily.

If the light angle variation is along the vertical direction (with no variation along the horizontal direction), the difference in responses of the diode pair B and D (or A and C) will help us to determine the angles.

B. Simulations

In order to verify correctness of the theoretical formulation constructed earlier, we performed simulations based on the derived equations. The result is plotted in Fig. 9 and shows the relationship between difference response produced by unshaded areas (A_{ushC} - A_{ushD}) of photodiodes as a function of incident light angle. The difference in the unshaded area has a direct correlation with the amount of intensity captured by the photodiodes. As the response produced by the photodiodes are dependent on the intensity of light falling on them, the difference in their response will be linear since the difference in their unshaded area is linear.

FDTD simulations further consolidate the concept and help to determine the parameters that lead to an appreciable output response. The light angle was varied from $-45°$ to $+45°$ along the horizontal direction and diode responses were recorded. Fig. 10 shows the Electric field profile for negative ($-40°$) and positive ($+40°$) angles. The difference response is plotted in Fig. 11 and it shows a linear variation in recorded intensity as the angle is varied.

Although the response produced by QPC is linear, its sensitivity to angle variation is low. Angular sensitivity is defined as the strength of response for small changes in angle. If the strength of response is large for a small change in angle, the angular sensitivity is high. This means that the QPC can unambiguously resolve angles that are far apart, but not the ones that are close together.

Comparing Eq. (12) and Eq. (13) we see that the parameter T_M is responsible for angular sensitivity. Larger the value of T_M, greater is the difference in the response produced by adjacent photodiodes. Fig. 12 shows the FDTD simulation results for different metal thicknesses. 1x refers to the thickness of lower metal layers (typically metal 1 to metal 5 or metal 6 depending on the process) in a CMOS metal stack, 4x and 12x refers to four times and twelve times the thickness of the lower level metal layers. These metal layers constitute the upper level metal stack of the CMOS process. The number of metal layers and the thickness of the layers vary from process to process. As can be seen from the figure, as the thickness of the metal layer increases, the slope of the response (sensitivity) increases. Consequently, using a higher level metal layer leads to a more sensitive QPC and hence better angle resolution.

In order to determine the effect of metal shading on the sensitivity of the response, we performed FDTD simulations by varying the amount of metal area that covers the photodiodes. Metal area over the photodiode was varied from 30% to 70% and the resulting values were plotted (Fig. 13). As can be seen, larger the area covered by metal over the photodiode, higher is the sensitivity.

Since QPC is based on the concept of metal shading, we expect the response produced by it to have no dependence on the wavelength of incident light. Fig. 14 shows a 3 dimensional variation of electric field intensity as a function of wavelength and incidence angle for the difference response produced by a pair of QPC pixels (for angle variation along a single direction - horizontal or vertical). Large positive angles show bright red color and large negative angles show bright blue color indicating linear variation of intensity with incident angles. For small angles around 0°, the response shows no changes with wavelength. However, there is a small wavelength dependence at large positive and negative angles due to diffraction effects around metal edges.

IV. Track-and-Tune Angle Detection Technique

The two angle detecting pixel structures seen earlier (Talbot pixels and QPC) have their own merits and demerits. Talbot pixels have good sensitivity for small changes in angle, but are highly dependent on the wavelength, grating pitch and number of gratings on top of the photodiode. Furthermore, angle resolution needs pixels with different angle sensitivities and their directional dependence necessitates need for different directional gratings (horizontal, vertical and diagonal). QPC, on the other hand, is unaffected by the numerous factors that plague Talbot pixels, but have low angular sensitivity. A compromise is achieved by combining the positives that both the pixel structures have to offer.

The track-and-tune angle detection technique [22] makes use of QPC to provide coarse estimate of angle and Talbot pixels for fine angle resolution. The principle is depicted in Fig. 15. Say, suppose the angle of incident light is 15°, the QPC will coarsely identify that the angle is around 15°, but will be unable to pin point the correct value. Now, once we know where the angle is located, we can use that particular segment (S_1 - S_2) of the periodic cosine Talbot pixel response

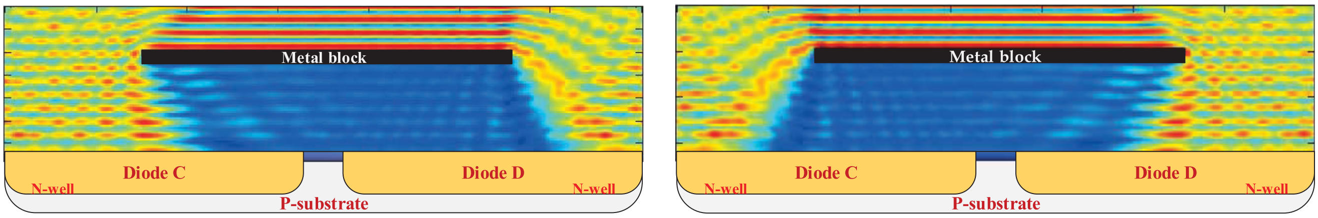

(a) (b)

Fig. 10. FDTD simulations showing electric field profiles for a pair of pixels in a quadrature pixel cluster. (a) Negative angle ($\alpha = -40°$). (b) Positive angle ($\alpha = +40°$).

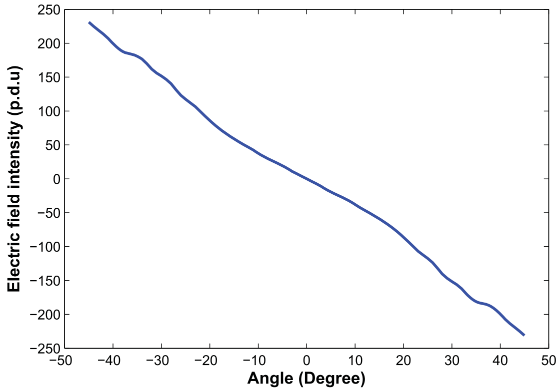

Fig. 11. Variation in intensity as a function of incident angle for two adjacent photodiodes in a quadrature pixel cluster.

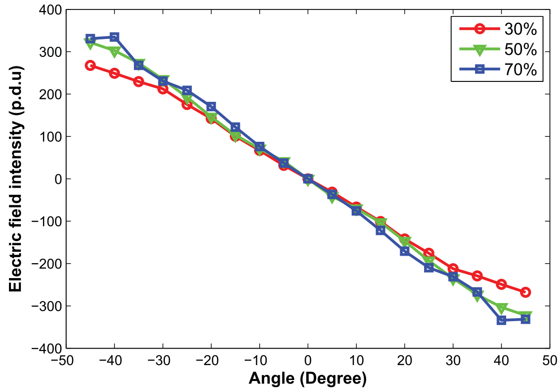

Fig. 13. Quadrature pixel response as a function of incident angle for varying metal widths.

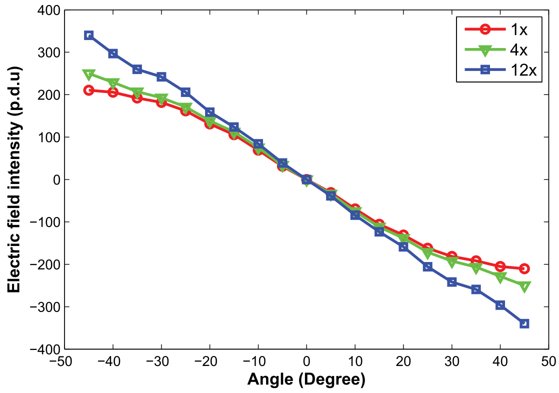

Fig. 12. Quadrature pixel response as a function of incident angle for varying metal thickness.

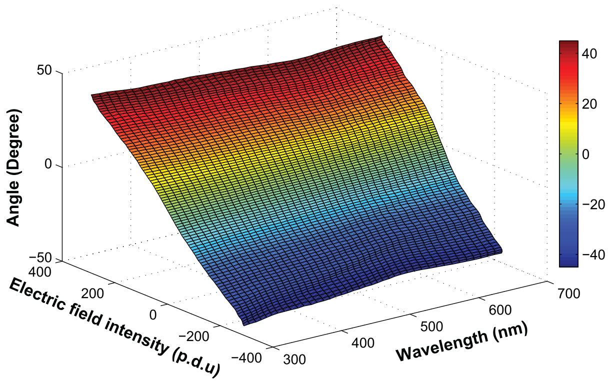

Fig. 14. Three-dimensional plot showing difference-intensity variations as a function of angle and wavelength for a pair of pixels in a quadrature pixel cluster.

to pin point the angle. Hence, this technique only requires a Talbot group with angular sensitivity pixels of a single kind and a single QPC for accurately determining the incidence angles. Since QPC can detect vertical and horizontal angles, a single QPC can be shared with a vertical (having vertical grating) and a horizontal (having horizontal grating) Talbot group.

V. Sensor Architecture

The proof-of-concept sensor occupies an area of 1.6 mm $\times$ 1 mm and was fabricated in 65 nm GlobalFoundries mixed-signal CMOS process. Fig. 16 shows the sensor architecture along with the chip microphotograph. The pixel array is made up of 12 $\times$ 10 macro pixel clusters. Fig. 17 shows the internal architecture of a macro pixel cluster. Each macro pixel cluster consists of 4 macro pixels, which share a switched capacitor amplifier. Each macro pixel, in turn, is made up of 13 distinct pixel types as shown in the figure. Pixels 1 to 8 are Talbot pixels and pixels 9 to 12 are QPC's. Pixel 13 is an ordinary pixel which captures only intensity. Table I lists the different pixel types along with the metal configuration used on top of the photodiodes. The pixels have been configured to produce difference response. Pixels 1, 2 and 3, 4 produce Talbot difference response for vertical angle variations (because of

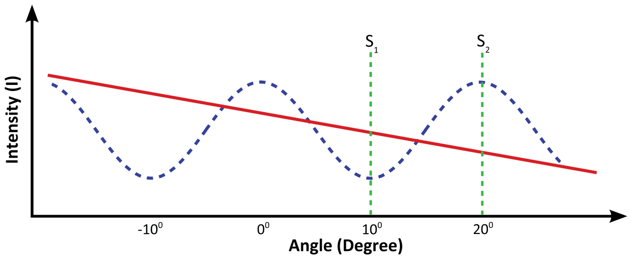

Fig. 15. Technique illustrating angle detection using Talbot and QPC pixel responses.

horizontal grating). Pixels 5, 6 and 7, 8 produce Talbot difference response for horizontal angle variations (because of vertical grating). Pixels 9, 10 and 11, 12 produce linear difference response for horizontal angle variations. Finally, pixels 9, 11 and 10, 12 produce linear difference response for vertical angle variations. Fig. 17 also shows ideal pixel responses.

The switched capacitor amplifier produces difference response and it amplifies the same by a factor of 2. It is made up of a 7T OpAmp and consists of two switches at the input. The input switches are made up of transmission gates (TG) and contain additional dummy transistors for cancelling the charge injection (CIC) into the input capacitor when TG is turned off. It produces output in accordance with Eq. (18).

$$\mathrm{V_{OUT}} = \mathrm{V_{REF}} - \frac{2C}{C}(\mathrm{V_{PIXELB}} - \mathrm{V_{PIXELA}}) \qquad (18)$$

N-well/p-sub photodiode makes up the light sensing part of the pixel. Each pixel measures 12.5 μm $\times$ 9 μm and consists of 5 transistors. Three transistors along with the photodiode make up the conventional 3T APS structure and the other two transistors are for selection control. Each pixel additionally contain a n-well guard ring and a p-sub guard ring for better isolation. The effective photo sensing area is 6 μm $\times$ 6 μm, giving rise to a fill factor of 32%.

All the primary and secondary Talbot pixel gratings have a pitch of 0.76 um. This pitch was selected in order to produce optimum response for a design wavelength of 532 nm in vacuum. M5 metal layer acts as the primary grating and M1 metal layer acts as the secondary grating. For QPC, metal block is made of metal layer M5 and it covers 50% of the photodiode.

Fig. 18 shows the sensor control signals. “PIX RST” is an active low reset signal, which resets the pixel to VDD. At the end of “PIX RST”, the pixel begins to integrate light. At the end of the exposure period, “EXP OVER” signal is raised high. Once the “EXP OVER” signal is asserted high, one of the pixels (pixel A) receives a “PIX SEL” signal. The pixel then sends its integrated voltage to the SC amplifier. After a “CLK” cycle delay, the “SELA” signal is asserted high and the pixel charge is then stored in the input capacitor. At the same time the output is reset to V_{REF}. When “SELA” goes low, another pixel (pixel B) receives the “PIX SEL” signal. This pixel voltage goes to the second input of the SC amplifier. After a cycle delay “SELB” is asserted high and the SC amplifier produces an output after a certain delay. When the output

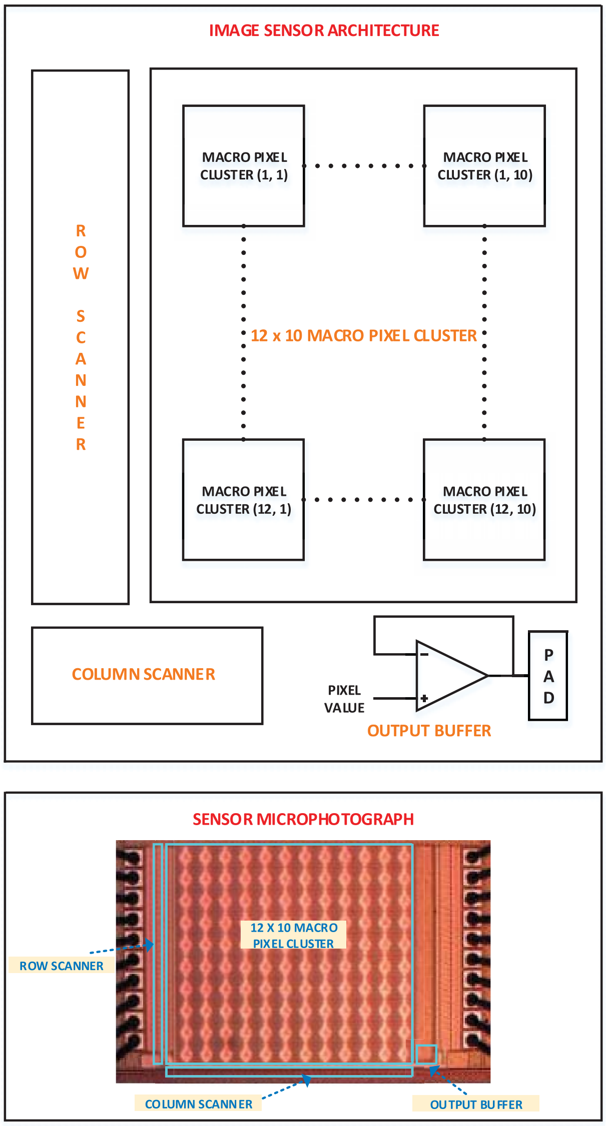

Fig. 16. Sensor architecture along with chip microphotograph.

is ready, “VALID” signal is asserted high and the external ADC samples the output for conversion and downstream processing.

Important sensor characteristics are listed in Table II. Photodiode sensitivity is the strength of signal developed by the pixel per unit of input optical energy and is measured for intensity pixels. Angular sensitivity on the other hand, is a measure of the angle dependent pixel response and is measured for Talbot and QPC pixels.

VI. Results and Discussion

Fig. 20 shows the conceptual diagram of the test setup which consists of a sun simulator and a rotary board. The sun simulator (Fig. 21(a)) emits highly collimated light rays toward the sensor. The sensor is mounted on a rotary table (Fig. 21(b)), which allows for its rotation with an accuracy of 5°. The sun simulator emits light over a broad

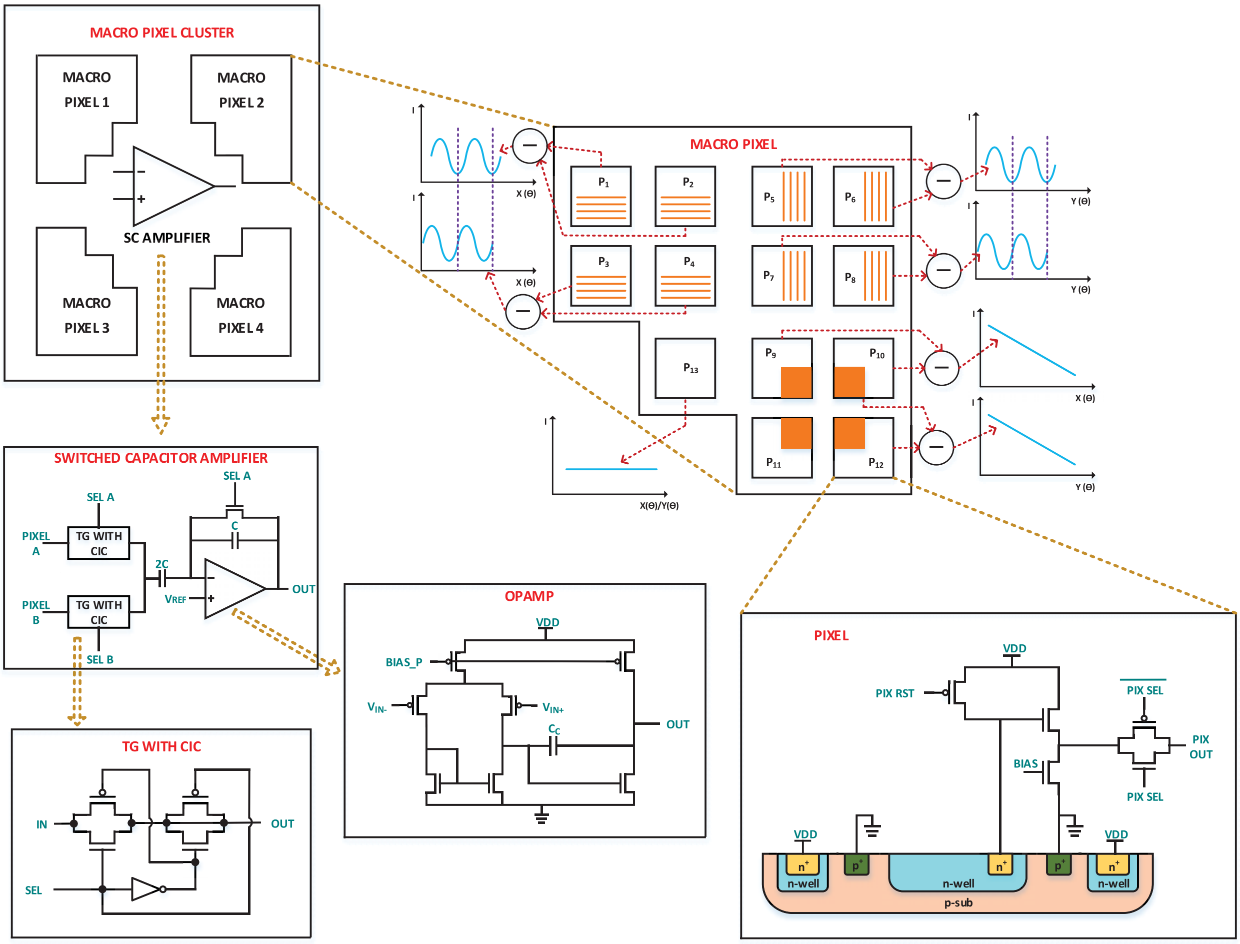

Fig. 17. Sensor schematic showing the various structural components of the fabricated sensor. The various pixel types and their ideal responses are also shown (refer Table I for different pixel types).

TABLE I
PIXEL TYPES IN A MACRO PIXEL

Pixel	Metal configuration	Grating offset	Response type
P_1	Horizontal grating	0	Cosine - offset 0
P_2		d/2	Cosine - offset π
P_3		d/4	Cosine - offset $\pi/2$
P_4		3d/4	Cosine - offset $3\pi/2$
P_5	Vertical grating	0	Cosine - offset 0
P_6		d/2	Cosine - offset π
P_7		d/4	Cosine - offset $\pi/2$
P_8		3d/4	Cosine - offset $3\pi/2$
P_9	Metal block	-	Linear
P_{10}		-	Linear
P_{11}		-	Linear
P_{12}		-	Linear
P_{13}	No metal	-	Intensity

range of wavelengths covering the entire visible spectrum (300 nm–700 nm).

The image sensor is interfaced with an external serial ADC and requires regulated 3.3 V and 1.2 V to function properly. The sensor communicates with the PC through an Opal Kelly XEM 3010 integration board which consists of a FPGA for generating control signals, a SDRAM for storing output digital values from the ADC and many other peripheral circuits.

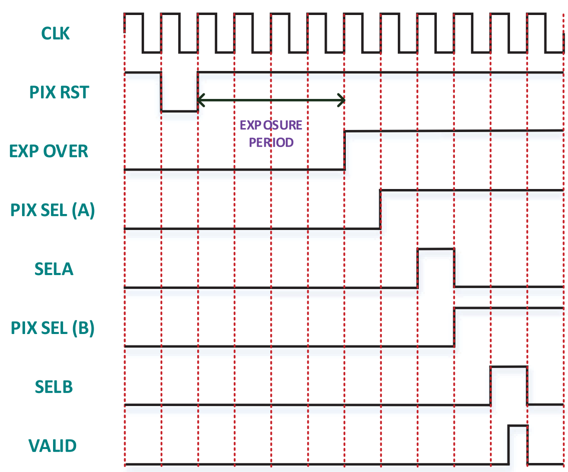

Fig. 18. Sensor control signals.

Measurements were made, first without any optical filter over the sensor and then with a 500 nm filter that has a passband of ± 2 nm around 500 nm. For both cases, angles

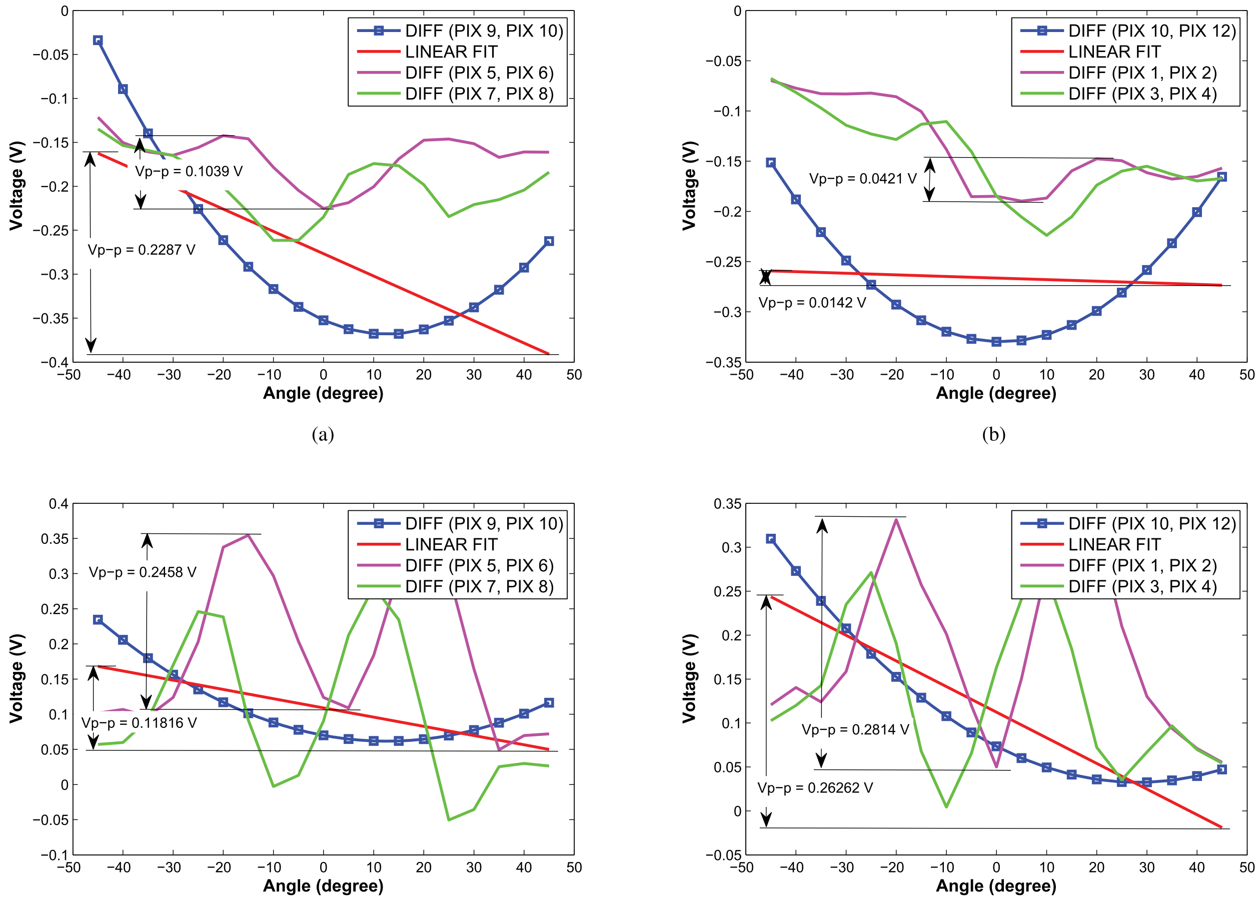

(a) (b) (c) (d)

Fig. 19. Plot of measured pixel responses as the incidence angle is varied from $-45°$ to $+45°$. Different pixel types and ideal responses are shown in Fig. 17 and Table I. (a) Pixel response without filter (angle variation along X direction). (b) Pixel response without filter (angle variation along Y direction). (c) Pixel response with 500 nm filter (angle variation along X direction). (d) Pixel response with 500 nm filter (angle variation along Y direction).

were first varied along the horizontal (X) direction and then along the vertical (Y) direction. Average values of pixels of similar kind over the entire pixel array are plotted (Fig. 19). Fig. 19(a) and Fig. 19(b) show the pixel responses without any optical filter and Fig. 19(c) and Fig. 19(d) show the pixel responses with a 500 nm optical filter on top of the sensor. In all the cases, it is the difference response that has been plotted. The various pixel types shown in the plots are given in Fig. 17 and Table I. The experimental QPC values were subjected to a polynomial fit of degree 2 and it is this data that has been plotted.

Possible reasons for parabolic nature of the QPC response curves are light refraction from multiple dielectric layers in the CMOS metal stack and shadowing of pixels from metal layers in the periphery of the pixels. The anomaly can be corrected to a certain extent to obtain linear response by using the intensity pixel response (scale the intensity pixel response and subtract it from QPC pixel response). The "LINEAR FIT" line shows the general linear trend of the QPC response.

In order to determine the angle of incident light, we first look at the QPC response to get a coarse estimate. We then corroborate the result by looking at the Talbot pixel response, which also refines the angle to a finer value. As an example consider Fig. 19(a), which shows the QPC and Talbot pixel response for angle variation along the X (horizontal) direction. We can use any one of the curves (either DIFF (PIX5, PIX6) or DIFF (PIX7, PIX8)) for fine angle measurement, as both contain the same information, albeit with a small offset. Let us consider DIFF (PIX5, PIX6) for angle detection. Fig. 22 shows the experimental determination of angle. Only relevant waveforms from Fig. 19(a) have been reproduced in Fig. 22.

In the figure "Measurement instance" represents the time instant at which the angle information is captured. At this instant, QPC pixels have voltage corresponding to the coarse angle value and Talbot pixels have voltage corresponding to the fine angle value. Since the angular sensitivity of QPC pixels are low, their angular resolution is low. For the present case, let us suppose that they can distinguish between angles over a 10° increment between $-45°$ to $+45°$. This is indicated by the "Coarse angle range" in the figure. In order to determine the exact angle value within a 10° angular range we need fine resolution. This is provided by Talbot pixels that can distinguish fine angles, say over a 5° increment (5° is just

TABLE II
IMPORTANT SENSOR PARAMETERS

Parameter	Value
Technology	65 nm, CMOS mixed-signal process
Chip size	1.6 mm x 1 mm
Pixel size	12.5 μm x 9 μm
Fill factor	32 %
Pixel structure	3T APS
Pixel power consumption	10.13 μW
Dark current	58 mV/sec
Temporal noise	0.54 mV
Dynamic range	71 dB
Full well capacity	68,000 e^-
Conversion gain	28.5 $\mu V/e^-$
Photodiode Sensitivity	0.53 V/lux-sec
Angular Sensitivity at $\lambda = 500$ nm (Talbot pixel)	14.07 mV/deg
Angular Sensitivity at $\lambda = 500$ nm (QPC pixel)	2.918 mV/deg
Angular Periodicity (QPC pixel)	20 deg
Array size	(12 x 10) x (4 x 13)
Supply voltage	3.3 V analog; 1.2 V digital

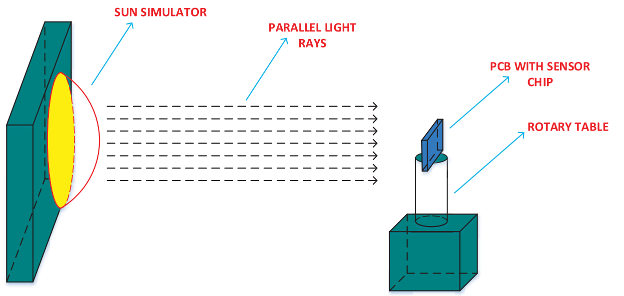

Fig. 20. Conceptual diagram of the test setup.

an example, the actual value is limited by the accuracy of the measurement setup and readout circuits). This is indicated by "Fine angle range" in the figure.

Suppose we have light at an angle around 10°, the QPC pixel indicates that the angle is 10° (considering that the angle resolution capability of QPC pixel is 10°). This could either be the actual angle or the actual angle might be somewhere near this angle. We then proceed to see the response produced by Talbot pixel. Since Talbot pixels have greater angular sensitivity, they can resolve angles with a much finer resolution, 5° or even 1°. Fig. 22 shows Talbot pixels with an angular resolution of 5°. In the absence of a reference angle, such as that provided by QPC pixel, there would be ambiguities in the measurement of angles using only the Talbot pixel response. For example, in Fig. 22, both $-5°$ and $+5°$ have approximately the same voltage values. This would require additional Talbot pixels with different angular sensitivities to resolve the ambiguity [9].

In the present case, we use guidance provided by the QPC response to aid in determination of incident angles. Since the angle from QPC response is 10°, we can consider the Talbot response around this angular range to determine the exact angle. By examining the Talbot response we see that the actual angle is in fact $+5°$ (considering that the angle resolution capability of Talbot pixel is 5°).

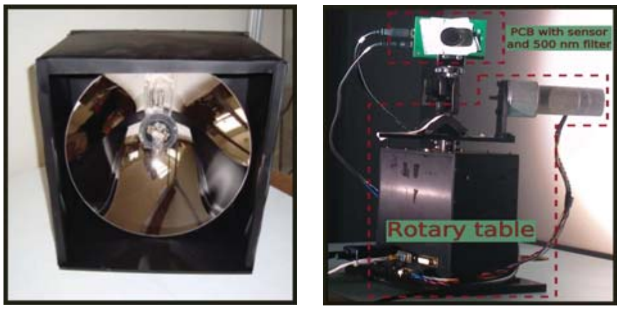

(a) (b)

Fig. 21. Test setup showing the sun simulator, PCB board (which houses the sensor) and rotary table. (a) Sun simulator. (b) Real test setup illuminated by the sun simulator.

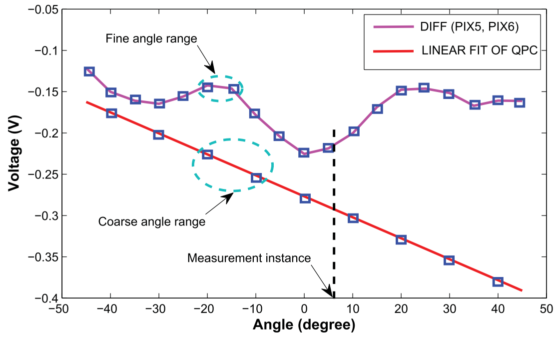

Fig. 22. Figure showing measurement of angle from experimental data.

The imaging scene generally contains light at different wavelengths. The wavelength dependent response produced by the Talbot only design makes it unsuitable for practical applications. The reduced response strength (Fig. 19(a) and 19(b)) without filters prove this point. In the presence of a broadband source emitting light over a broad range of wavelengths, the grating produces self-images at a particular depth, dependent on the characteristic wavelength. The response perceived by the photodiode for such a source will be the resultant of all the characteristic responses. Hence a solution consisting of coarse angle tracking by QPC and fine angle tuning by Talbot pixel is the easiest way out. The technique can be employed satisfactorily for a wide variety of applications.

VII. Conclusion

We have presented a new pixel type, called the Quadrature Pixel Cluster (QPC), that is capable of capturing the incident angle information. Only a set of four pixels are needed to determine angle along the horizontal and vertical directions. Since the angle is encoded in the form of linear variations in intensity, simple electronic circuits are sufficient to decode the angle information. Furthermore, we have proposed a new technique based on the QPC to accurately decode the angle information. According to the new technique, QPC can be used to detect coarse angles and Talbot pixels can then be employed for fine angle resolution. This strategy tremendously reduces the complexity of the Talbot-only design. Prior work uses 32 Talbot pixels to resolve angles along horizontal and vertical directions. The new technique on the other hand reduces this requirement to 13 pixels. We have demonstrated that by using the new technique, angles in the range from $-35°$ to $+35°$ can be distinctly distinguished. This technique can be readily used for fine angle measurements and will further simplify many problems associated with 3D image reconstruction and post capture image refocus.

REFERENCES

[1] A. Gershun, "The light field," *J. Math. Phys.*, vol. 18, pp. 51–151, 1939.
[2] E. H. Adelson and J. R. Bergen, "The plenoptic function and the elements of early vision," in *Computational Models of Visual Processing*. Cambridge, MA, USA: MIT Press, 1991, pp. 3–20.
[3] M. Levoy and P. Hanrahan, "Light field rendering," in *Proc. 23rd Annu. Conf. Comput. Graph. Interact. Techn. SIGGRAPH*, 1996, pp. 31–42.
[4] S. J. Gortler, R. Grzeszczuk, R. Szeliski, and M. F. Cohen, "The lumigraph," in *Proc. 23rd Annu. Conf. Comput. Graph. Interact. Techn. SIGGRAPH*, 1996, pp. 43–54.
[5] K. Marwah, G. Wetzstein, Y. Bando, and R. Raskar, "Compressive light field photography using overcomplete dictionaries and optimized projections," *ACM Trans. Graph. (Proc. SIGGRAPH)*, vol. 32, no. 4, pp. 1–11, 2013.
[6] A. Veeraraghavan, R. Raskar, A. Agrawal, A. Mohan, and J. Tumblin, "Dappled photography: Mask enhanced cameras for heterodyned light fields and coded aperture refocusing," *ACM Trans. Graph.*, vol. 26, no. 3, p. 69, 2007.
[7] G. Lippmann, "Epreuves reversibles donnant la sensation du relief," *J. Phys. Theory Appl.*, vol. 7, no. 1, pp. 821–825, 1908.
[8] K. Fife, A. El Gamal, and H.-S. P. Wong, "A multi-aperture image sensor with 0.7 um pixels in 0.11 um CMOS technology," *IEEE J. Solid-State Circuits*, vol. 43, no. 12, pp. 2990–3005, Dec. 2008.
[9] A. Wang and A. Molnar, "A light-field image sensor in 180 nm CMOS," *IEEE J. Solid-State Circuits*, vol. 47, no. 1, pp. 257–271, Jan. 2012.
[10] A. Molnar and A. Wang, "Light field image sensor, method and applications," U.S. Patent 20 110 174 998, Jul. 21, 2011.
[11] A. Wang, P. Gill, and A. Molnar, "Angle sensitive pixels in CMOS for lensless 3D imaging," in *Proc. IEEE Custom Integr. Circuits Conf. (CICC)*, Sep. 2009, pp. 371–374.
[12] K. Fife, A. El Gamal, and H.-S. P. Wong, "A 3Mpixel multi-aperture image sensor with 0.7 um pixels in 0.11 um CMOS," in *IEEE Int. Solid-State Circuits Conf. (ISSCC) Dig. Tech. Papers*, Feb. 2008, pp. 48–594.
[13] A. Wang, P. R. Gill, and A. Molnar, "An angle-sensitive CMOS imager for single-sensor 3D photography," in *IEEE Int. Solid-State Circuits Conf. Dig. Tech. Papers (ISSCC)*, Feb. 2011, pp. 412–414.
[14] K. Fife, A. El Gamal, and H.-S. P. Wong, "A 3D multi-aperture image sensor architecture," in *Proc. IEEE Custom Integr. Circuits Conf. (CICC)*, Sep. 2006, pp. 281–284.
[15] C. Koch, J. Oehm, and A. Gornik, "High precision optical angle measuring method applicable in standard CMOS technology," in *Proc. ESSCIRC*, Sep. 2009, pp. 244–247.
[16] C. Koch, J. Oehm, J. Emde, and W. Budde, "Light source position measurement technique applicable in SOI technology," *IEEE J. Solid-State Circuits*, vol. 43, no. 7, pp. 1588–1593, Jul. 2008.
[17] H. F. Talbot, "Facts relating to optical science. No. IV," *Philosoph. Mag.*, vol. 9, no. 56, pp. 401–407, 1836.
[18] L. Rayleigh. (1881). XXV. On copying diffraction-gratings, and on some phenomena connected therewith. *Philosoph. Mag. J.*, vol. 11, no. 67, pp. 196–205. [Online]. Available: http://www.tandfonline.com/doi/abs/10.1080/14786448108626995
[19] M. Testorf, J. Jahns, N. A. Khilo, and A. M. Goncharenko. (1996). Talbot effect for oblique angle of light propagation. *Opt. Commun.*, vol. 129, no. 34, pp. 167–172. [Online]. Available: http://www.sciencedirect.com/science/article/pii/0030401896001319
[20] D. S. Mehta, S. K. Dubey, C. Shakher, and M. Takeda. (2006, Oct.). Two-wavelength talbot effect and its application for three-dimensional step-height measurement. *Appl. Opt.*, vol. 45, no. 29, pp. 7602–7609. [Online]. Available: http://ao.osa.org/abstract.cfm?URI=ao-45-29-7602
[21] E. Hecht, *Optics*, 4th ed. Reading, MA, USA: Addison-Wesley, 2002.
[22] V. Varghese, X. Qian, S. Chen, and S. ZeXiang, "Linear angle sensitive pixels for 4D light field capture," in *Proc. IEEE Int. SoC Des. Conf. (ISOCC)*, Nov. 2013.

Vigil Varghese (S'13) received the B.E. degree in electrical and communication engineering from Visvesvaraya Technological University, Bangalore, India, in 2009. He is currently pursuing the Ph.D. degree at the School of Electrical and Electronic Engineering, Nanyang Technological University, Singapore. He was an Associate CAE with Synopsys, Bangalore, and a Senior Design Automation Engineer with and a Senior Design Automation Engineer with Standard Micro Systems Corporation (acquired by Microchip), Chennai.

His current research is on CMOS image sensors for computational photography, which encompasses areas, such as integrated optics, VLSI design, and 3-D algorithms.

Xinyuan Qian received the B.S. degree in electrical engineering from the Shanghai Jiao Tong University, Shanghai, China, in 2006, and the M.S. degree in electrical engineering from the Technical University of Munich, Munich, Germany, in 2008. He is currently pursuing the Ph.D. degree at the School of Electrical and Electronic Engineering, Nanyang Technological University, Singapore.

His current research interests include high dynamic range CMOS image sensors and smart vision sensors for space applications.

Shoushun Chen (M'05) received the B.S. degree from Peking University, Beijing, China, the M.E. degree from the Chinese Academy of Sciences, Beijing, and the Ph.D. degree from the Hong Kong University of Science and Technology, Hong Kong, in 2000, 2003, and 2007, respectively.

He held a Post-Doctoral Research Fellowship with the Department of Electronic and Computer Engineering, Hong Kong University of Science and Technology, for one year after graduation. From 2008 to 2009, he was a Post-Doctoral Research Associate with the Department of Electrical Engineering, Yale University, New Haven, CT, USA. In 2009, he joined Nanyang Technological University (NTU), Singapore, as an Assistant Professor.

Dr. Chen serves as a Technical Committee Member of Sensory Systems, the IEEE Circuits and Systems Society, an Associate Editor of the IEEE *Sensors Journal*, the Program Director (smart sensors) of VIRTUS, and the IC Design Centre of Excellence at NTU. His research interests include smart vision sensors, motion detection sensors, energy-efficient algorithms for bio-inspired vision, and analog/mixed-signal VLSI circuits and systems.

Shen ZeXiang received the B.Sc. degree in physics from Jilin University, Changchun, China, and the Ph.D. degree from King's College, University of London, London, U.K. He is a Professor with the School of Physical and Mathematical Sciences, and the Co-Director with the Centre for Disruptive Photonics Technologies, Nanyang Technological University (NTU), Singapore. He was awarded the NTU Nanyang Award for the Research and Innovation in 2009, and the Gold Medal for the Research Excellence by the Institute of Physics, Singapore, in 2011.

His main research interests include near-field Raman microscopy, plasmonics, spectroscopic study of graphene and 2-D materials, stress and strain study of Si nano devices, graphene-based electrode materials for battery, and supercapacitor applications.

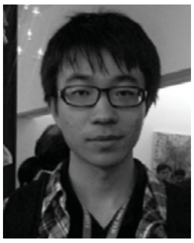

Tao Jin received the M.Sc. degree in optics from the South China Normal University, Guangzhou, China, in 2011. He is currently pursuing the Ph.D. degree at the School of Electrical and Electronic Engineering, Nanyang Technological University, Singapore. His research interests include Mid-IR plasmonic photonic devices and Mid-IR quantum cascade lasers with beam combing.

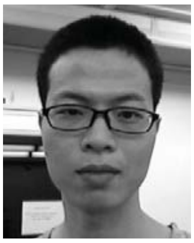

Liang Guozhen was born in Fu Jian, China, in 1986. He received the B.S. degree in physics from the University of Science and Technology of China, Hefei, China, in 2010. He is currently pursuing the Ph.D. degree in microelectronics at the School of Electrical and Electronic Engineering, Nanyang Technological University, Singapore. His current research interests include the development of high performance terahertz quantum cascade lasers, terahertz plasmonics, and integrated graphene devices.

Qi Jie Wang received the Ph.D. degree in electrical and electronic engineering from the Nanyang Technological University (NTU), Singapore, in 2005, where he worked for two years after the graduation. From 2007 to 2009, he joined the School of Engineering and Applied Science, Harvard University, Cambridge, MA, USA, as a Post-Doctoral Researcher. In 2009, he was a Joint Nanyang Assistant Professor with the School of Electrical and Electronic Engineering and the School of Physical and Mathematical Sciences, NTU.

His current research interests are to explore theoretically and experimentally nano-structured semiconductor and fiber-based materials, and nanophotonic devices with an emphasis on investigating the fundamental properties of semiconductor and fiber lasers, and nanophotonic devices in the infrared frequency regimes.